

N 7 3 - 2 0 9 4 1

~~N 7 3 - 2 0 9 4 1~~

**NASA TECHNICAL
MEMORANDUM**

NASA TM X-68212

NASA TM X-68212

**CASE FILE
COPY**

**EXHAUST PLUME AND CONTAMINATION CHARACTERISTICS
OF A BIPROPELLANT (MMH/N₂O₄) RCS THRUSTER**

by Ernie W. Spisz, Robert L. Bowman, and John R. Jack
Lewis Research Center
Cleveland, Ohio 44135

TECHNICAL PAPER for presentation at
Seventh JANNAF Plume Technology Conference
Redstone Arsenal, Alabama, April 3-5, 1973

EXHAUST PLUME AND CONTAMINATION CHARACTERISTICS OF

A BIPROPELLANT (MMH/N₂O₄) RCS THRUSTER

by Ernie W. Spisz, Robert L. Bowman, and John R. Jack

National Aeronautics and Space Administration
Lewis Research Center
Cleveland, Ohio

ABSTRACT

Results are presented for three recent experiments in a series of thruster contamination experiments made in the liquid helium-cooled environmental facility of the NASA Lewis Research Center. The general objective of this study is to investigate the contaminating effects encountered on various materials, surfaces, and components, due to the exhaust products from a 5-pound thrust, bipropellant (MMH/N₂O₄) thruster. This paper is limited to the following topics: (1) the angular distribution of plume effects around the periphery of the thruster as established by transmittance changes of quartz samples over the wavelength range from 0.2 to 2.0 micrometer, (2) mass deposition rates at a specific location as measured with a quartz crystal microbalance for three different experiments, (3) quadrupole mass spectrometer measurements of the exhaust products over the mass number range from 12 to 75, (4) infrared transmittance measurements of contaminated samples for the wavelength range from 2.5 to 15 microns, and (5) infrared transmittance measurements of residue collected from the thruster nozzle for signature identification of the residue.

The plume distribution effects indicated a general decrease in transmittance as the angle between the sample and the nozzle centerline increased. A favorable comparison was obtained between the angular distribution of the transmittance and an approximation to the plume mass density distribution for angles up to approximately 56°. Two samples located at angles of ±85° however indicated greater transmittance changes than predicted by the trends of the plume mass flow distribution. The quartz crystal microbalance measurements indicated not only large changes in mass deposition rates between the three different experiments but also daily as well as day to day changes during a given experiment even though engine operating parameters were not changed. The data obtained from the quadrupole and infrared transmittance measurements indicated that identification of the contaminant may be possible but it will be extremely difficult to apply these techniques to provide quantitative data which can be related to contamination effects.

INTRODUCTION

The problems and concerns of spacecraft contamination are well recognized as indicated by the extensive coverage provided to the subject at recent conferences (refs. 1 to 4). As spacecraft systems increase in complexity and missions increase in duration, the possibility of encountering contamination effects which can seriously compromise or even destroy functional or experimental components also increases. Reviews of the possible effects, the seriousness of the contamination problem, and the need for performing experiments to document the contaminating effects are presented in

references 5 and 6. Definitive experiments which contribute to the understanding of the contamination problem are extremely difficult to perform. Sources of contamination, their subsequent effects, and the many parameters which must be considered and controlled have many facets and generally tend to be unique for a given situation or application.

In general, contamination studies consist of (1) the measurement of changes or damage due to the contaminant on the operational characteristics of surfaces, materials, or components, (2) the identification of the degrading contaminant and its source, (3) the definition of the conditions and the parameters which control the extent and formation of the contaminant, and (4) a study of the methods to eliminate or minimize the contaminant or contaminant effects. These four areas present a challenging array of experimental problems that tax limits of available equipment and instrumentation even though much progress has been made on new measurement techniques (e.g., refs. 7 to 9).

Of the many possible sources of contamination that occur, contamination due to the exhaust plumes of RCS thrusters presents one of the more serious threats to many spacecraft surfaces and experiments. Yet only very limited quantitative data are available in this area. The paucity of data is due to the experimental difficulties encountered in simulating the proper environment and the inherent problems associated with the sophisticated measurements and control systems required to obtain worthwhile data. For example, in order to eliminate the interaction between the environmental facility and the plume contamination source, it is necessary to resort to large clean vacuum facilities having large pumping speeds for all gases including hydrogen. This invariably requires large liquid helium cryopumped systems and large distances between the experiment and the measuring instrumentation with the attendant instrumentation wiring and signal conditioning problems. In addition, compromises must frequently be made in the experimental procedure due to facility characteristics, and the logistics and economics of the cryogenic fluids required for operating the facilities.

The Lewis Research Center has available a large supply of recoverable liquid helium so that thruster contamination studies can be performed with proper simulation. During the past several years we have been involved in making general studies on contamination effects due to RCS thrusters. (Results from previous tests performed in this general study have been reported in refs. 10 and 11.)

The purpose of this paper is to present the results obtained in the most recent series of studies being carried out at the Lewis Research Center on contamination from a 5-pound thrust MMH/N₂O₄ bipropellant engine. The data presented were obtained from three different experiments that were conducted during the past year. The results will concentrate primarily on the distribution of contamination effects as determined by transmission changes of quartz samples and the characteristics of the contaminant as measured with quartz crystal microbalances, a quadrupole mass spectrometer, and an infrared spectrometer. The results for "damage" effects are being reported at this meeting in two companion papers (refs. 12 and 13).

FACILITY

The experiments were carried out in the 2x4 meter liquid-helium-cooled space simulation chamber described in reference 14. The engine and the experiment package are located within the facility as shown in figure 1. The engine is a pressure-fed bipropellant single/doublet unit with a stainless steel radiation-cooled nozzle. The fuel is MMH and the oxidizer is N_2O_4 . The thruster is fired in a horizontal direction toward the liquid helium-cooled wall. During thruster firing a gaseous argon leak is introduced into the simulator to enhance the ability of the tank wall to cryopump hydrogen obtained during thruster firing (see ref. 14 for a discussion of this effect). The engine is generally fired in a pulse mode of operation with an ON-time less than 200 msec, an OFF-time greater than 100 msec, and in a series of pulses corresponding to a total ON time of less than 500 msec. The pulse mode type of operation is of interest because most RCS thrusters operate with this duty cycle.

Included within the facility at various locations are fast response ambient pressure gauges to monitor the response and pumping characteristics of the facility. With liquid helium-cooled walls, the facility pressure is less than 1×10^{-9} torr during nonfiring periods. During thruster firing periods the tank pressure increases to 6×10^{-7} torr due to the imposed gaseous argon leak to enhance hydrogen pumping. At the moment of thruster firing, the tank pressure increases momentarily to 5×10^{-5} torr but within 3 minutes returns to the steady value of 6×10^{-7} torr.

A fast scan quadrupole mass spectrometer is located on the test section wall behind the nozzle exit plane and approximately $1\frac{1}{2}$ meters above the engine centerline to measure the constituents of combustion gases. A 60° magnetic sector mass spectrometer is included within the facility instrumentation at the instrument ring for facility monitoring and residual gas analysis.

Solar simulation is provided by the carbon arc lamp and optics section of the facility. The optics section consists primarily of an optics tower housing a lenticular lens system to provide good beam uniformity and a 1-meter diameter collimating mirror to provide a 1-meter illuminated test plane. The resulting beam has an intensity of approximately 0.7 solar constant and closely approximates the solar spectrum.

EXPERIMENTS

A summary comparison of the three different experiments for which results will be presented is shown in table I. Basically the experiments are similar in that the effects of contaminants from the exhaust plume of the MMH/ N_2O_4 5-pound thruster for pulse mode type operation on various surfaces and components were investigated. Most of the test hardware and instrumentation for each experiment is similar except for Experiment 3 which included a new sample pallet and the extensive application of quartz crystal microbalances (QCM) to define the distribution of deposited mass within the plume and the back flow regions. Figures 2(a), (b), and (c) show a schematic drawing of the test plane and a description of the samples and instrumentation which is of interest for each of the three experiments.

Experiment 1 was primarily a long duration experiment as indicated by the 49-day period over which the experiment extended. The primary purpose of this experiment was to obtain "damage" data on various materials and components for extended thruster firing periods. During the 49-day period of this experiment the engine was fired for a total of 4468 (50 msec) pulses and accumulated a total firing exposure time of 223.7 seconds without breaking the vacuum of the facility. The sample pallet consisted primarily of white and black thermal control paints, quartz and mirrored surfaces, silicon solar cells, and an assortment of other materials such as aluminum, molybdenum, kapton, and mylar. In addition to the pallet samples, nine samples were mounted on the engine centerline height and perpendicular to the plume flow direction to establish a plume profile in terms of measured effects on the transmittance of quartz samples. Two quartz crystal microbalances were also included in the experiment; the QCM's are located as shown in figure 2(a) and are mounted so the crystal surface corresponds to the elevation of the sample surfaces. The QCM's are 5×10^6 Hz crystals that are mounted in water-cooled crystal holders that are maintained at approximately supply water temperature (20° C). QCM 1 malfunctioned early in the experiment; consequently, data will be presented only for QCM 2. The quadrupole mass spectrometer included in the experiment was also inoperative.

Experiment 2 was very similar to experiment 1 except that the duration of the experiment was shorter and consisted of much less exposure to the thruster plume. The engine was fired on four separate days and accumulated 1241 (50 msec) pulses and a total exposure time of 62 seconds. The primary objective of experiment 2 was to establish a damage distribution profile around the thruster as measured by transmittance or reflectance changes for 20 "sting-mounted" samples. A series of pallet samples were included for comparison to experiment 1 data. Two quartz crystal microbalances were also included in this experiment. QCM 1 was mounted at the nozzle exit plane and facing in the direction of plume discharge to measure possible plume back-flow. QCM 2 was mounted in exactly the same location as QCM 2 in experiment 1.

The quadrupole mass spectrometer was again included in experiment 2 and many scans were obtained during the experiment. A container was located below the nozzle and at the nozzle exit plane to collect any residue or drippings which might fall directly from the nozzle. The residue was used for both chemical and infrared analysis at the completion of the experiment.

Experiment 3 was a departure from experiments 1 and 2 in that the pulse mode of thruster operation was changed from the 50 millisecond ON-time pulse used previously to a 14-millisecond ON-time pulse. Experiment 3 consisted of 5375 (14 msec) firing pulses and provided a cumulative exposure of 75.5 seconds. The primary objective of experiment 3 was to establish the degradation of solar cells to the short pulsing period and to establish the distribution of mass deposition around the thruster as indicated by the use of 13 QCM's in the experiment. Much of the data from experiment 3 have not been completely analyzed and only a limited amount of data for one QCM (4) will be presented.

RESULTS AND DISCUSSION

Plume Distribution Effects. - In experiments 1 and 2 various passive samples were arranged in a horizontal plane around the thruster axis and normal to the exhaust flow direction in order to establish the angular distribution of contamination effects on quartz and mirrored surfaces. The samples were 1-inch in diameter and were placed around the engine at the engine centerline elevation and normal to the vector from the center of the nozzle exit area. The arrangement and number of samples were different for each experiment. The samples, the distance from the nozzle exit and the angle with the nozzle centerline are shown in figures 2(a) and (b).

In experiment 1, nine samples were mounted against an aluminum plate with only the front surface of the samples exposed. Six of the samples were fused quartz and were arranged to establish the contaminant effects on transmittance over an angle of $\pm 24^\circ$ from the engine centerline. The directional transmittance of the six fused quartz samples were measured over the wavelength range from 0.18 to 0.48 μm with a 1-meter 15° Robin mount scanning spectrometer having a 590 grooves per millimeter grating. The transmittance measurements were made by the sample-in/sample-out technique with the sample mounted at the inlet slit of the spectrometer. (See ref. 10 for details.) The transmittance measurements made by this method are referred to as directional because only the radiant energy which is transmitted through the sample and not scattered off the optical axis of the spectrometer is measured. The transmittance data for these samples is shown in figure 3. Data are not included for sample 109 because the back (or protected) surface of the sample became contaminated by the heavy contaminant layer flowing between the aluminum plate and its back surface. The contaminating layer on the exposed surface of these samples existed as a continuous film on all the samples rather than the discrete droplets which have been observed in previous experiments (refs. 10 and 12). The presence of a heavy contaminating layer corresponds with the significant decrease in transmittance shown in figure 3 especially for wavelengths below 0.3 μm . The thick contaminating layer resulted in essentially zero transmittance for wavelengths below 0.22 μm . The samples on the left side of the engine (105, 106, and 108) show a consistent trend of reduced effect as the angle between the sample and the nozzle centerline increases. The two samples on the right side of the nozzle axis (103 and 101) indicate a similar trend and also a somewhat smaller transmittance change than was measured on the left side of the nozzle centerline.

Experiment 2 was a more extensive study to establish the angular distribution of the contaminating effects on samples for angles as great as $\pm 85^\circ$ off the nozzle centerline. Each sample was individually supported (sting mounted) by clamping the sample around its outer rim so that both sides of the sample were exposed. The samples were aligned so the front surface was perpendicular to the nozzle radius vector. The exposed back surface of the sample was believed to introduce less of an effect than that encountered with the protected back surfaces used in experiment 1.

The directional transmittance measurements for the sting mounted samples are shown in figure 4(a) for samples on the left side of the nozzle centerline and in figure 4(b) for samples on the right side. A comparison

of transmittance measurements in figures 4(a) and (b) shows a smaller contaminating effect for the samples on the right side than on the left. This trend was also noticed to a lesser degree in figure 3 for the experiment 1 data. For the first three samples on both the left and right sides there is also a general indication of decreasing contamination effects as the angle between the sample and the nozzle axis increases. The samples located at angles of $\pm 85^\circ$ off the nozzle axis (samples 101 and 120) indicate greater contaminating effect than samples 104 and 117 which are at 56° . It should be noted that the distance between the sample and nozzle center varies for each sample and the data should be interpreted in terms of both distance and angle. The extent of the contaminating effects for the samples at 85° is particularly surprising. Large transmittance changes were measured for wavelengths less than $0.3 \mu\text{m}$ despite two contrary indications, viz. (1) the visual appearance of the samples showed only a slight contaminant haze with no noticeable liquid droplets and (2) QCM1 which was located in this area indicated very little mass deposition (less than the $0.01 \mu\text{g}/\text{cm}^2$ resolution capability of the instrument).

The magnitude of the contaminating effect for the samples near the nozzle axis was also considerably more than was expected for this experiment for the relatively short (62 sec) exposure to thruster firing. The contaminant effect on these samples is as large as that measured for the samples of experiment 1 in which the total exposure to thruster firing was considerably longer (223.7 sec).

In figures 5(a) and (b) the hemispherical transmittance measurements of the samples are shown for the wavelength range from 0.31 to $2.5 \mu\text{m}$. These measurements were made with an integrating sphere, lithium fluoride prism spectrometer system (ref. 12). The changes in hemispherical transmittance are due primarily to absorption effects and are less than the changes measured for the directional transmittance. The data for the samples on both the left and right side of the engine centerline indicate a generally consistent trend of decreasing effect with increasing angle off the nozzle axis. There are exceptions in the data but these are considered to be minor. The change in transmittance for these samples is negligible for wavelengths greater than $0.8 \mu\text{m}$.

The angular distribution of the effects of the contaminating layer on the transmittance of the samples has been related to the plume flow field by considering the transmittance in terms of the Lambert-Bouguer Law of absorption (ref. 15) and the plume flow field as defined by the approximate relationship given in reference 18. According to the Lambert-Bouguer Law, the transmittance of a uniform absorbing layer of thickness x is

$$\tau_c = e^{-k_c(\lambda)x_c}$$

where $k_c(\lambda)$ is the absorption coefficient of the absorbing layer and is generally wavelength dependent and consequently the transmittance must also be considered monochromatically. The $k(\lambda)x$ product is referred to as the optical density of the layer. If the uniform, absorbing layer is deposited on a clean but absorbing substrate (as in the case of the contaminated samples to be considered), the transmittance of the contaminated substrate

(τ_{cs}) can be determined in terms of the transmittance of the clean substrate, τ_s (and neglecting minor front surface reflection effects) as

$$\frac{\tau_{cs}}{\tau_s} = e^{-k_c(\lambda)x}$$

For the samples that are being considered here, the contaminating layer is not uniform but composed rather of discrete droplets. The analogy, however, to the uniform layer model is appropriate provided that the absorption coefficient and thickness values are understood to be effective (or integrated) values.

If it is now assumed that the effective optical density of the contaminant is proportional to the mass flow density in the exhaust plume in the region of the sample, the effective optical density and plume mass flow are related by (ref. 16).

$$-k_c x = \ln\left(\frac{\tau_{cs}}{\tau_s}\right) \propto \left(\frac{r_o}{r}\right)^2 e^{-\beta^2(1-\cos\theta)^2}$$

The coordinates of the sample location in the plume are r and θ , r_o is an arbitrary reference radial distance generally taken along the nozzle axis, and β^2 is a function of the specific heat ratio of the combustion products and the nozzle area ratio (ref. 16).

Figure 6 presents the correlation of the hemispherical transmittance measurements from experiment 2 (shown in figs. 5(a) and (b)) for the two wavelengths of 0.32 and 0.42 μm . The transmittance data are presented as $(r/r_o)^2 \ln(\tau_{cs}/\tau_s)$ in order to normalize transmittance effects to a common radius so that angle between sample and nozzle centerline is the only independent parameter. The hemispherical transmittance data are suited for this correlation because the measurements include only absorption as required in the Lambert-Bouguer Law. The angular distribution of the transmittance data compares favorably with the plume mass distribution curve for a specific heat ratio of 1.2. This value for the specific heat ratio corresponds to the value used in reference 17 where the specific heat ratio for a MMH/ N_2O_4 thruster was calculated to range from 1.20 to 1.28 through the plume. The data follow the predicted trend except for the two samples which were located at $\pm 85^\circ$. The transmittance data for these samples are at least one order of magnitude higher than the predicted value indicating that the simplified approximations for the mass distribution have been extended beyond their limits of applicability and edge effects have become important.

Reference 18 also shows much larger deposition rates than predicted by Hill and Draper for large angles off the nozzle centerline.

Quartz Crystal Microbalance Measurements. - Quartz crystal microbalances (QCM's) are being used extensively for flight and ground test contamination experiments (refs. 19 to 22). These devices are capable of highly sensitive, real-time measurements of the mass depositing or leaving the surface of the sensing crystal. The crystals of the QCM units used herein

have a diameter of 0.5 inch, a thickness of 0.01 inch, and an exposed surface of approximately 1 cm^2 . The crystals are cut on the AT-plane, are silver coated and have natural oscillating frequencies of 5×10^6 Hertz. The crystal frequency is dependent on both the net mass deposited on the crystal and the crystal temperature. Water cooling is provided for the crystal holder to minimize the temperature effect on crystal frequency. The sensitivity of the QCM measuring system, assuming a deposit material density of unity, corresponds to an average contamination thickness of 1 \AA or a mass change of $0.01 \text{ micrograms/cm}^2$. References 20 and 21 present additional detail regarding QCM characteristics and their applications to contamination monitoring.

Data will be presented for one QCM from each of the three experiments. (QCM 1 was inoperative in experiment 1 and only limited data were obtained for QCM 1 for experiment 2.) Thirteen QCM's were included in experiment 3; however, the data for only one QCM are available at this time. Referring to figure 2, the QCM's for which data will be presented are designated 2, 2, and 4 for experiments 1, 2, and 3, respectively. These three QCM's are identical units. The location of the QCM for experiments 1 and 2 are also identical, while in experiment 3 the location is nearer the engine axis and closer to the nozzle exit plane.

Figures 7, 8, and 9 show typical QCM data obtained using strip chart recorders that were operated continuously during each of the three runs to measure contamination deposition and evaporation rates during thruster firing periods. The general character and response of the QCM's for the three runs are all qualitatively similar. The recorder trace is a stepwise curve that shows a net increase in mass with time. A description of the phenomena being indicated by the QCM measurements can be made by referring to figure 7(a). This figure illustrates the response of QCM 2 in experiment 1 over a continuous recording period of approximately one hour. The step change in the data occurs every seven minutes and coincides with the moment of thruster firing. The thruster firing consists of eight 50 millisecond firing pulses with 100 millisecond between each pulse. The total pulsed firing period occurs over an elapsed time of 1.2 seconds. The instantaneous step increase in the trace is due to the deposition of exhaust plume products on the crystal surface. The gradual decrease in the trace after the initial step increase is due to subsequent evaporation or sublimation of the deposited exhaust plume materials. For the specific step increases shown in figure 7(a), the mass addition is approximately $0.6 \text{ micrograms/cm}^2$ per second of engine firing (0.4 sec). During the seven minutes between firing periods some of the deposited mass evaporates or sublimates from the crystal surface at a rate of between 0.02 to $0.04 \text{ microgram/cm}^2$ per minute as indicated by the decrease in the recorded trace. The net mass which remains on the crystal surface just prior to the next firing period is approximately $0.3 \text{ microgram/cm}^2$. A net mass deposit of 3.0 \mu gr was obtained for the 1-hour period shown and results in a net mass addition rate of approximately $0.05 \text{ microgram/cm}^2/\text{minute}$. All of the QCM data exhibit this typical character, however the magnitude of the changes are different for the different experiments.

Table II lists the approximate average increase of the initial mass addition, the evaporation or sublimation rates during nonfiring periods,

and the net mass addition to the crystal surface for a number of selected days during the experiment. The results of the QCM data from the other experiments are also included in table II for comparison. For a given experiment and thruster operating parameters the QCM results for the various days are similar. However, there are some differences during a given day as well as differences from day to day. For experiment 1 the initial mass addition covers a range from 0.4 to 1.5 micrograms/cm² (a rate for the 0.4 sec firing period is 1.0 to 3.75 micrograms/cm²/sec) and the net mass addition covers a range from 0.5 to 0.7 micrograms/cm²/minute. There were no large deviations in the QCM data for this experiment even though the experiment was carried out over an extended period of time.

The response of QCM 2 in experiment 2 shown (fig. 8) is similar to the data obtained in experiment 1. However, the initial mass deposition rates are less and the day-to-day response of the QCM was not as stable or consistent as that for experiment 1 data. The initial mass change during engine firing is only 0.1 to 0.3 micrograms/cm² (or only 0.25 to 0.75 micrograms/cm²/sec of engine firing) and a net change of 0.042 to 0.070 micrograms/cm² per engine firing occurred. The only experimental parameter which changed between experiments 1 and 2 was the increase in the crystal holder water temperature from approximately 2° C (winter period) for experiment 1 to 15° C (summer period) for experiment 2. It is doubtful that this slight change in water temperature could account for the large change in deposition rates which occurred between the two experiments.

The response of QCM 4 in experiment 3 (fig. 9) also shows the typical "increasing step" character with each thruster firing. The day-to-day comparison of the recorded trace for this QCM was also generally consistent during thruster firing periods. The initial rise or mass deposition during thruster firing was approximately 1 to 4 micrograms/cm² per engine firing (a deposition rate at 2.8 to 11.5 µg/cm²/sec of engine firing) and a net change over the firing period of approximately 0.1 to 1.0 micrograms/cm². The much larger deposition rates measured for experiment 3 as compared to experiment 1 and 2 may be attributed somewhat to the different location. The primary difference, however, is due to the different pulse mode of operation (14 msec-ON, 100 msec-OFF, 25 pulses) for experiment 3 as compared to the (50 msec-ON, 100 msec-OFF, 8 pulses) for experiments 1 and 2. Even though the total ON-time of 350 milliseconds for experiment 3 is comparable to the 400 millisecond ON-time for experiments 1 and 2, the higher mass deposition rates for experiment 3 are indicative of the increased contamination to be expected for short ON-time pulses.

It is of interest to consider the two recorder traces shown in figure 10 which indicate two unusual events which occurred during experiments 2 and 3. The trace in figure 10(a) shows the response of QCM 2 in experiment 2 during the thruster firing period of the third firing day of the experiment. The step-wise increase at each engine firing is evident but there is a decrease in the net mass deposition rates. The net loss in mass during the firing period is due to the greater evaporation loss of existing material on the QCM as compared to the deposition rate due to thruster firing. It is possible that this may be due to long term temperature or electronic drift in the crystal measuring systems; however, frequent and repeated checks of crystal performance during nonfiring periods indicated excellent stability over long periods of time.

Figure 10(b) shows the response of QCM 4 from experiment 3 when engine firing and solar simulation occurred simultaneously. As can be noted, the imposed radiation causes very erratic behavior in crystal response due to temperature effects on the crystal characteristics and increased evaporation of the existing mass on the crystal surface. Consistent mass deposition rates could not be obtained when solar radiation occurred simultaneously with thruster firings. In experiments 1 and 2, solar simulation occurred only during nonfiring periods where the resultant effect was to reduce the mass remaining on the crystal surface.

Some limited data for QCM 1 of experiment 2 were obtained intermittently at approximately 1 hour intervals during the firing period. The net mass addition to this crystal is also shown in table II and indicates only a slight mass addition during the second firing day and no measurable mass addition during the last two firing days of the experiment. The conclusion drawn from these data is that the plume backflow as measured by QCM 1 is apparently small and less than the resolution (approximately $0.01 \mu\text{g}/\text{cm}^2$) of the QCM measuring system. Even though the mass deposition rates were small, the significant changes measured in directional transmittance may be of importance for space applications.

Quadrupole Mass Spectrometer Measurements. - A quadrupole mass spectrometer was included in the experiments in an attempt to identify the engine exhaust products causing contamination effects and, if possible, to correlate the exhaust products from different engine operating conditions to contamination effects. A general description of a quadrupole mass spectrometer and its potential for contaminant analysis is presented in references 23 and 24.

The spectrometer is attached to the tank wall (fig. 1) approximately 1.5 meters above the thruster nozzle. The spectrometer is encased in a 6-inch diameter stainless steel can which has a 1-inch diameter sampling port facing upward. No data are available from experiments 1 and 3 since the quadrupole was inoperative in these experiments. The results from experiment 2 are presented to indicate the type of information that can be obtained with this instrument.

Spectrometer scans over the mass number (m/e) range from approximately 4 to 80 are shown in figures 11(a) to (d). The scans are intended only for qualitative comparisons to illustrate differences between various scans taken during different operating conditions. Figure 11(a) was obtained prior to any engine firing, figure 11(b) is a scan one minute prior to the 20th pulse on the first day of firing, figure 11(c) was obtained 60 seconds after the 20th pulse was fired, and figure 11(d) is a background scan taken five days after the first day's firing. The scan speeds were 30 seconds for figures 11(a) and (d) and 3 seconds for figures 11(b) and (c).

Figure 11(a) shows the initial background spectra with major mass number peaks at 29, 41, 43, 55, and 57 representing, according to reference 25, the presence of hydrocarbons. There are minor peaks at mass numbers 15, 17, 30, 44, and 46, indicating possibly the presence of NO^{++} , NH_3 , NO , N_2O , MMH , and NO_2 which are known to be exhaust constituents for $\text{MMH}/\text{N}_2\text{O}_4$ thrusters. The presence of these various mass numbers in the background spectrum is probably due to contamination remaining from previous thruster firings and

cleaning solvents used to remove the contaminants from the facility.

Figures 11(b) and (c) were made at much lower sensitivity levels than 11(a) in order to obtain a scan as soon as possible before and after the thruster was fired and before most of the exhaust constituents had been pumped by the liquid helium walls of the facility. Because of the reduced sensitivity the detailed structure of the background is not evident and only the very predominant peaks can be seen. In figure 11(b) the prominent peak at 40 and the secondary peak at 20 indicate A^+ and A^{++} due to the argon leak which is used continuously during the thruster firing period. The result of thruster firing can be noted by comparing figures 11(b) and (c). An obvious difference between figures 11(b) and (c) can be seen by comparing the change in peak height of mass numbers 14, 15, 16, 17, and 18 relative to the stable peak height at mass number 40. The increase in relative peak heights at these mass numbers can be attributed to the exhaust gases CO^{++} , N_2^{++} , N, NO^{++} , O, O_2^{++} , NH_3 , OH, and H_2O . However, of more importance, is the change in peak height noted for mass numbers 30, 31, 45, and 46 which could indicate the presence of NO, CH_3NH_2 , $C_2H_5NH_2$, and NO_2 and MMH. If so, incomplete combustion may have occurred for the pulse operating mode and these products may be the contaminants in the plume causing optical degradation.

A final scan of the residual tank background is shown in figure 11(d) and can be compared with figure 11(a). The primary differences are the relative increase in mass 14 and the relative decrease in the intensity of mass number 29 relative to 28, the presence of appreciable 32 (which is attributed to N_2H_4 or CH_3OH rather than O_2), and the large increase in mass 46 indicating again possibly unburnt MMH or residual NO_2 .

Due to the difficulties encountered in operating the mass spectrometer in our facility, the rapidly changing tank background immediately after thruster firing and the large number of chemical compounds contributing to the mass spectra, no positive identification of exhaust products causing contamination was possible. Although a comparison of the mass spectra obtained from different engine operating conditions may give some insight into engine operation contributing to contamination effects, we expect that such a correlation will be very difficult to make. Our experience at this time pretty much agrees with the conclusion drawn in reference 23 that the utilization of a mass spectrometer to determine residue composition is extremely difficult even with a great deal of effort.

Infrared Spectrometer Measurements. - Ex-situ infrared transmittance measurements were made for wavelengths from 2.5 to 15 μm for (1) liquid collected directly from the thruster nozzle to obtain a "signature" of the contaminant and (2) three "sting-mounted" samples (102, 107, and 109) that were located in and directly contaminated by the plume.

Figure 12 shows the infrared spectra of the dark brown, viscous liquid collected directly below the nozzle. The spectra were obtained with a double-beam, filter grating spectrometer with the liquid on a sodium chloride (NaCl) and also on a potassium bromide (KBr) plate. On the NaCl substrate, absorption bands are centered at 2.9 and 7.4 μm with other bands appearing at 5.65 and 6.7 μm as well as between 9 and 13 μm . Spectra of the liquid on the KBr substrate show similar band structure; however, there are

some differences noted in the two spectra. These differences as well as the overall spectra are consistent with data shown in reference 25 for residue collected in the outer edges of the exhaust plume from the firing of a 1-pound thrust MMH/N₂O₄ engine. The spectra in reference 25 were further compared and found to be identical to the spectra obtained from laboratory prepared MMH/HNO₃. The identification of the contaminant from the spectra presented herein is not this positive. Even though a similarity does exist between these spectra and that of reference 25 additional analysis is required before a positive identification can be made.

An elemental chemical analysis was also made on the collected material; the results of the analysis are shown in table III and are compared with similar analyses from reference 25. Although the chemical analysis of the sample is similar it is also different enough, especially in percent of nitrogen, to suggest the possibility of a different substance. This possibility can occur considering the different locations from which the material was collected.

Figure 13 presents the infrared spectra for the sting-mounted NaCl sample (109) and the KRS-5 sample (107). These samples are contaminated directly from plume exhaust products which may differ chemically from the material collected from the nozzle exit. The spectra in figure 13 are not as well defined as the previous spectra because the amount of contaminant is much less. The primary absorption bands at 2.9 and 7.4 μ m are easily detected and can be compared with the spectra in figure 12. Again it should be noted that the KRS-5 sample spectra (similar to the effect noted with the KBr spectra) differs slightly from spectra obtained with the NaCl sample. Thus it appears that contamination effects are affected by the substrate and care must be taken to insure comparable substrates if the data are to be compared.

In figure 14 the infrared spectra of the two sting-mounted NaCl samples 102 and 109 are compared for wavelengths up to 6 μ m to illustrate the influence of sample location. No significant differences were noted in the spectra for wavelengths greater than 6 μ m. The extent of the absorption is considerably less for sample 102 than for sample 109 at a wavelength of 2.9 μ m. The decreasing effect with increasing angle is consistent with the plume mass distribution and the results obtained for the fused silica samples.

The infrared spectra obtained herein indicate a number of items worth summarizing: (1) the spectra for the material collected as drippings from the nozzle exit appears to be similar to spectra for collected exhaust products obtained by others in the fields, (2) the use of sting-mounted samples in the exhaust plume to collect exhaust contaminants for signature identification requires more material than deposited in our exposure test or more sophisticated spectrometer measuring techniques, and (3) narrow band measurements at wavelengths of 2.9 and 7.4 μ m may be useful for in-situ, real time measurements of contaminating effects or possible correlations with mass deposition rates. It is also apparent from this study that relating infrared measurements to contamination effects is difficult as is the application of the quadrupole mass spectrometer measurements and that both techniques require a great deal of time, effort, and development if useful quantitative data are to be obtained.

CONCLUDING REMARKS

The conclusions which can be drawn from the data of the three experiments are as follows:

Plume Distribution Effects. - The effect of the plume contaminants on the transmittance of fused quartz samples located around the periphery of the engine increases as the wavelength decreases and also decreases as the angle between the sample location and nozzle centerline increases. The contaminant causes a significant reduction in directional transmittance for wavelengths below $0.3\ \mu\text{m}$. For the experiment with a total exposure time of 223 seconds, the directional transmittance of the sample was essentially zero for wavelengths below $0.22\ \mu\text{m}$. At wavelengths between 0.3 and $0.5\ \mu\text{m}$, the influence of exposure time greater than 62 seconds on directional transmittance was found to be small.

A comparison between the transmittance effects and an approximate description of the plume mass flow distribution indicated a reasonable correlation for the samples at angles up to ± 56 degrees. Two samples located at angles of ± 85 degrees showed larger transmittance effects than predicted by the mass flow distribution. These large transmittance changes at $\pm 85^\circ$ indicate possible plume back-flow effects which can be important considerations for space applications.

Quartz Crystal Microbalance Measurements. - Measurements of mass deposition rates during thruster firings were found to be different for each of the three experiments. The largest deposition rates were obtained for the shorter firing pulse (14 msec-ON time) operating mode.

Quadrupole Mass Spectrometer Measurements. - Problems were encountered in obtaining quadrupole measurements in two of the three experiments - measurements made during experiment 2 indicated major increases at mass numbers of 17, 18, 31, 45, and 46 immediately after thruster firing. These mass numbers suggest the presence of the compounds NH_3 , H_2O , CH_3NH_2 , $\text{C}_2\text{H}_5\text{N}_2$ or unreacted MMH which could condense on surfaces which are at temperatures below 250°K .

Infrared Spectrometer Measurements. - The spectra over the wavelength range from 2.5 to $15\ \mu\text{m}$ for material collected directly off the nozzle exit compared closely with spectra obtained by others working in this area. The spectra were similar to laboratory prepared MMH- HNO_3 ; however, a positive identification of the residue could not be made. Contaminant deposited on samples located directly in the exhaust plume was not sufficient for signature identification. These samples did indicate primary absorption bands at 2.9 and $7.4\ \mu\text{m}$ which could possibly be used for in-situ, real time contamination effect measurement or possible correlation to mass deposition rates.

REFERENCES

1. Symposium on Optical Contamination in Space, Aspen, Colorado, August 13-15, 1969.
2. Proceedings of the Fifth IES, AIAA, Space Simulation Conference, Gaithersburg, Maryland, September 14-16, 1970, Joseph C. Richmond, ed., National Bureau of Standards, NBS-SP-336, 1970.
3. Sixth AIAA Thermophysics Conference, Tullahoma, Tennessee, April 26-28, 1971.
4. Proceedings of the Sixth IES, AIAA, ASTM Space Simulation Conference, New York, New York, May 1-3, 1972, National Aeronautics and Space Administration, NASA SP-298, 1972.
5. Lyon, Warren C.: Monopropellant Thruster Exhaust Effects upon Spacecraft. J. of Spacecraft and Rockets, Vol. 8, No. 7, July 1971, pp. 689-701.
6. Cothran, C. A.; Greenburg, S. A.; and McCargo, M.: A Survey of Contamination of Spacecraft Surfaces. Paper No. 71-457, AIAA, April 1971.
7. Zwiener, James M.. Ground Contamination Monitoring Devices for the Apollo Telescope Mount. Paper No. 71-458, AIAA, April 1971.
8. Richmond, Robert G.; and Harmon, Henry N.: An Instrument for Real-Time Detection of Contamination in Space Environmental Test Chambers. Space Simulation. NASA SP-298, 1972, pp. 503-519.
9. Wolff, C. M.: Some New Techniques in Passive Contamination Analysis of Space Environment Simulation Chambers. Space Simulation. NASA SP-298, 1972, pp. 151-170.
10. Jack, J. R.; Spisz, E. W.; and Cassidy, J. F.: The Effect of Rocket Plume Contamination on the Optical Properties of Transmitting and Reflecting Materials. Paper No. 72-56, AIAA, January 1972.
11. Sommers, R. D.; Raquet, C. A.; and Cassidy, J. F.: Optical Properties of Thermal Control Coatings Contaminated by MMH/N₂O₄ 5-Pound Thruster in a Vacuum Environment with Solar Simulation. Paper No. 72-263, AIAA, April 1972.
12. Bowman, R. L.; Spisz, E. W.; and Jack, J. R.: Effects of Contamination on the Optical Properties of Transmitting and Reflecting Materials Exposed to a MMH/N₂O₄ Rocket Exhaust. Paper presented at 7th JANNAF Plume Technology Conference, Redstone Arsenal, Huntsville, Alabama, April 1973. NASA TM X-68204, March 1973.

13. Sommers, R. D.: Effect of Thruster Pulse Length on Thruster Exhaust Damage to S13G White Thermal Control Coatings. Paper presented at 7th JANNAF Plume Technology Conference, Redstone Arsenal, Huntsville, Alabama, April 1973.
14. Cassidy, J. F.: Space Simulation Experiments on Reaction Control System Thruster Plumes. Paper No. 72-1071, AIAA, November 1972.
15. Vasko, Antonin: Infrared Radiation. CRC Press, 1968.
16. Hill, Jacques A. F.; and Draper, James S.: Analytical Approximation for the Flow From a Nozzle into a Vacuum. J. of Spacecraft and Rockets, Vol. 3, No. 10, October 1966, pp. 1552-1554.
17. Webber, W. T.; Hoffman, R. J.; and Nunn, J. R.: Analysis of Potential Plume Contamination Effects Resulting from Two 300-Pound Bipropellant Engines Operating in a Satellite Environment. AFRPL-TR-72-66, Air Force Rocket Propulsion Laboratory, June 1972.
18. Chirivella, J. E.; Moyhihan, P. I.; and Simon, W.: Small Rocket Exhaust Plume Data. JPL Quarterly Technical Review, Vol. 2, No. 2, July 1972, pp. 90-99.
19. McKeown, D.; and Corbin, W. E., Jr.: Space Measurements of the Contamination of Surfaces by OGO-6 Outgassing and their Cleaning by Sputtering and Desorption. Space Simulation. Joseph C. Richmond, ed., NBS-SP-336, National Bureau of Standards, October 1970, pp. 113-127.
20. Chuan, R. L.: Particulate Contamination Measurement by Quartz Crystal Microbalance. Space Simulation. Joseph C. Richmond, ed. NBS-SP-336, National Bureau of Standards, October 1970, pp. 105-111.
21. Wallace, D. A.: Use of the Quartz Crystal Microbalance for Outgassing and Optical Contamination Measurements. Jour of Vacuum Sci and Tech, Vol. 9, No. 1, January/February 1972, pp. 462-466.
22. Kruger, Raymond; Scialdone, John J.; and Shapiro, Harold: A Comparison of Quartz Crystal Microbalance Measurements with Mass Spectrometer Determinations. Space Simulation. NASA SP-298, 1972, pp. 815-830.
23. Wolff, Calvin M.; and Ritter, Melvin L.: Contamination Measurements in Space Environment Chambers. Space Simulation. Joseph C. Richmond, ed. NBS-SP-336, National Bureau of Standards, October 1970, pp. 25-49.
24. Thekaekara, Matthew P.: Spacecraft Applications of Quadrupole Mass Spectrometry. Space Simulation. NASA SP-298, 1972, pp. 769-785.
25. Takimoto, H. H.; and Denault, G. C.: Combustion Residues from N_2O_4 -MMH Motors. SAMSO-TR-69-373, Space and Missile Systems Organization, September 15, 1969.

TABLE I. - SUMMARY OF EXPERIMENT CHARACTERISTICS

Experiment number	1	2	3
Time period	1/18/72 to 3/6/72	6/6/72 to 6/23/72	10/9/72 to 10/20/72
Total number of experiment days	49	20	12
Number of thruster firing days	16	4	6
Type of firing pulse	50 msec-ON, 100 msec-OFF, series of 8	50 msec-ON, 100 msec-OFF, series of 8	14 msec-ON, 100 msec-OFF, series of 25
Cumulated number of pulses	4468	1241	5375
Cumulated exposure time, sec	223.7	62.05	75.48
Number of passive pallet samples	34	33	6
Number of plume distribution samples	9	20	14
Number of solar cells	3	3	8
Number of QCM's	2	2	13
Quadrupole mass spectrometer	Inoperative	Yes	Inoperative
Infrared spectrometer	No	Yes	No

TABLE II. - SUMMARY OF QCM MASS DEPOSITION RATES

Day	Initial mass deposition rate		Evaporation or sublimation rate (between engine firing), $\mu\text{g}/\text{cm}^2/\text{min}$	Long term mass addition rate	
	Per engine firing $\mu\text{g}/\text{cm}^2$	Per sec of engine firing $\mu\text{g}/\text{cm}^2/\text{sec}$		Per engine firing, $\mu\text{g}/\text{cm}^2$	Elapsed time basis, $\mu\text{g}/\text{cm}^2/\text{min}$
Exp. 1 QCM 2	1	0.5-0.8	1.25-2.0	0.35	0.05
	2	0.4-0.8	1.0-2.0	.35	.05
	3	0.5-1.0	1.25-2.5	.49	.07
	4	0.8-1.5	2.0-3.75	.35	.05
Exp. 2 QCM 2	1	-	-	-	-
	2	0.1-0.2	0.25-0.5	0.056	0.008
	3	0.1-0.2	0.25-0.5	± 0.070	± 0.010
	4	0.1-0.3	0.25-0.75	.042	.006
Exp. 3 QCM 4	1	-	-	-	-
	2	1.5-3.0	4.30-8.5	0.56	0.08
	3	1.0-2.5	2.80-7.15	0.1-0.64	0.014-0.08
	4	2.0-4.0	5.6-11.5	1.0	0.14
Exp. 2 QCM 1	1	-	-	-	-
	2	-	-	0.014	0.002
	3	-	-	0.000	0.000
	4	-	-	0.000	0.001

TABLE III. - ELEMENTAL CHEMICAL ANALYSES OF COLLECTED MATERIAL

Element	Exp. 2 collected material	Ref. 25 residue	Ref. 25 calc. for MMH/HNO ₃
% Carbon	12.78	10.34	11.01
% Hydrogen	6.66	6.41	6.46
% Nitrogen	24.21	40.40	38.52

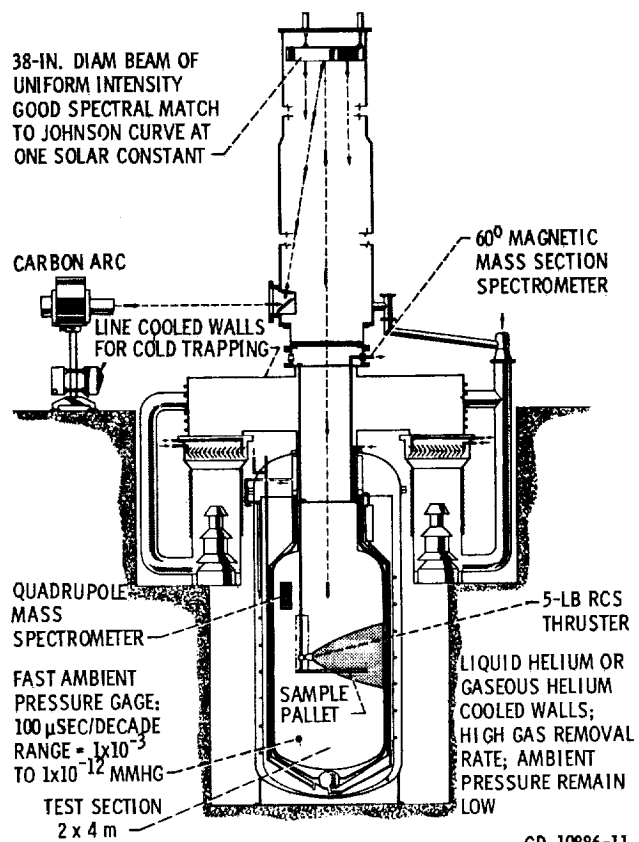
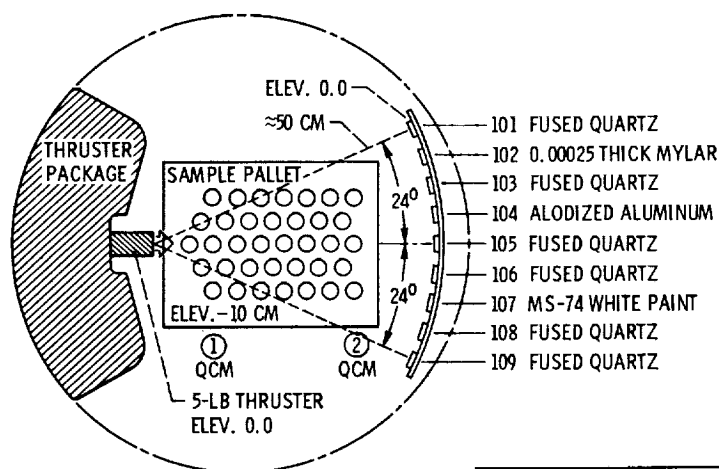
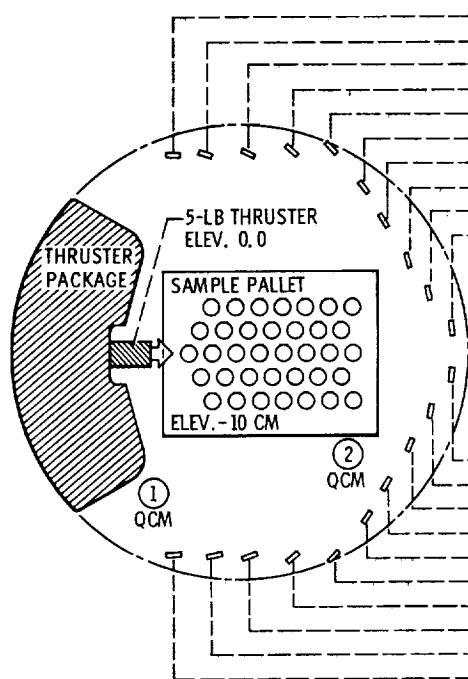


Figure 1. - In-situ rocket plume effects facility.



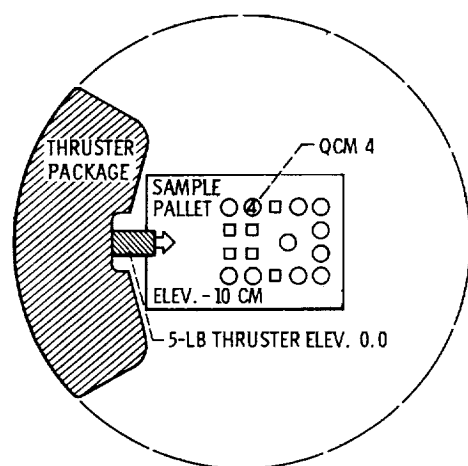
(a) EXPERIMENT 1.

SAMPLE NUMBER	ANGLE, DEG	DISTANCE, CM	SAMPLE MATERIAL
101	85	38	FUSED SILICA
102	74	39	SODIUM CHLORIDE
103	65	42	ALUMINUM
104	56	46	FUSED SILICA
105	49	51	BRASS
106	38	52	FUSED SILICA
107	30	51	KRS-5
108	20	51	FUSED SILICA
109	12	53	SODIUM CHLORIDE
110	4.5	55	FUSED SILICA



(b) EXPERIMENT 2.

SAMPLE NUMBER	ANGLE, DEG	DISTANCE, CM	SAMPLE MATERIAL
111	4.5	55	FUSED SILICA
112	12	53	FRONT SURFACE MIRROR
113	20	51	FUSED SILICA
114	30	51	FRONT SURFACE MIRROR
115	38	52	FUSED SILICA
116	49	51	FRONT SURFACE MIRROR
117	56	46	FUSED SILICA
118	65	42	PURE ALUMINUM
119	74	39	FRONT SURFACE MIRROR
120	85	38	FUSED SILICA



(c) EXPERIMENT 3.

Figure 2. - Experiment description.

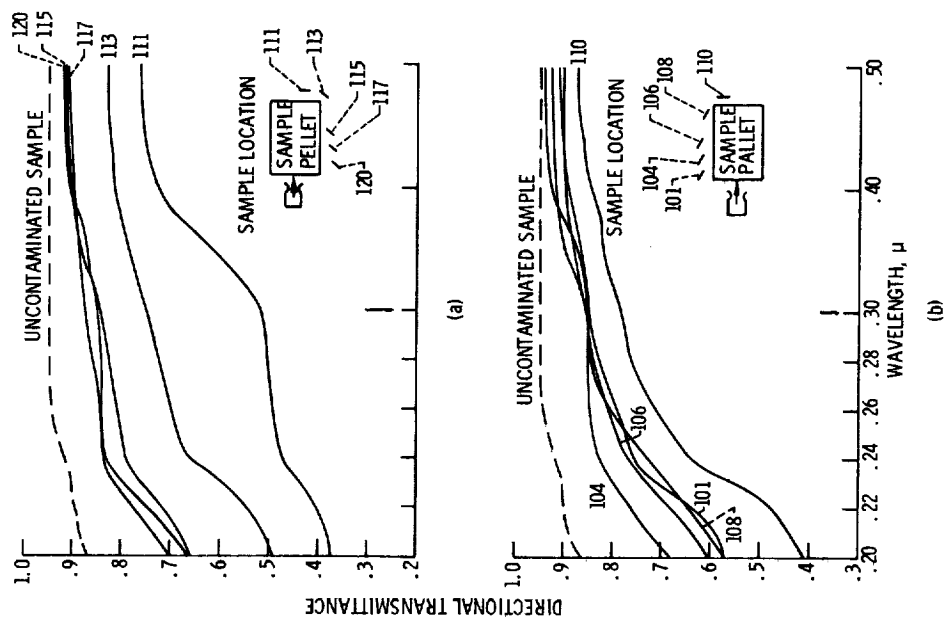


Figure 4. - Transmittance of contaminated fused silica samples. (Experiment 2, 62 seconds exposure.)

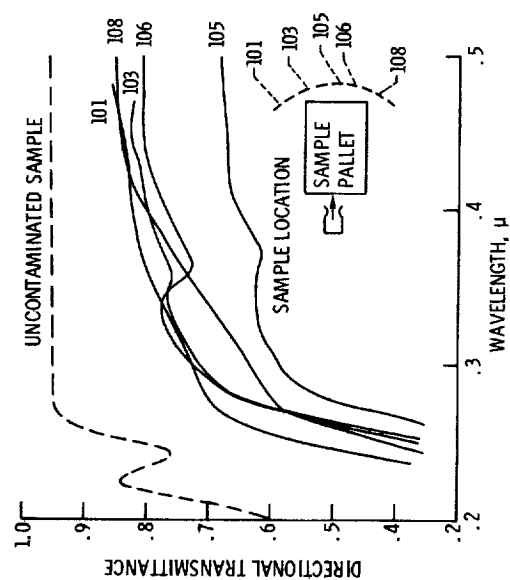


Figure 3. - Transmittance of contaminated fused quartz samples normal to plume. (Experiment 1, 223.7 seconds exposure.)

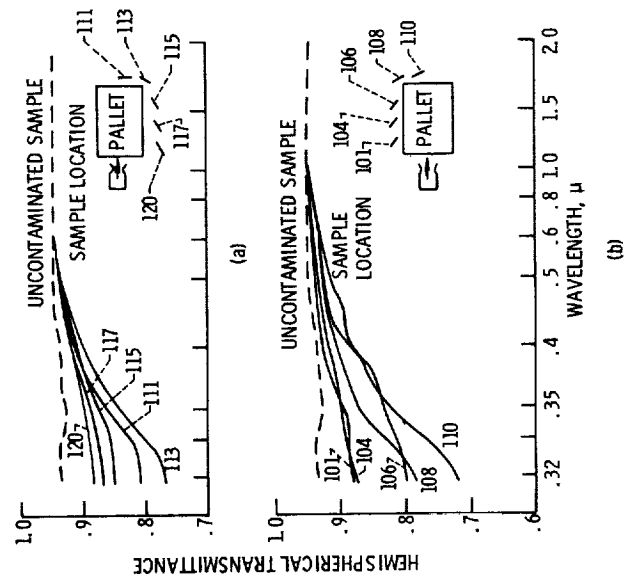


Figure 5. - Hemispherical transmittance of fused silica samples. (Experiment 2; 62 seconds exposure.)

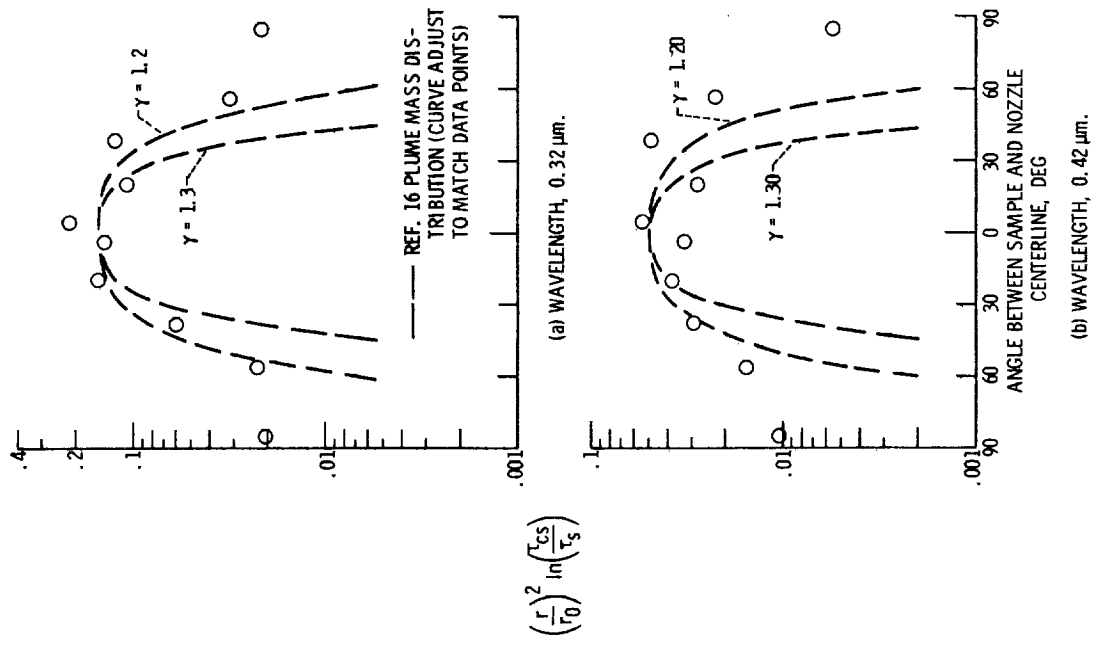


Figure 6. - Angular distribution of hemispherical transmittance (experiment 2).

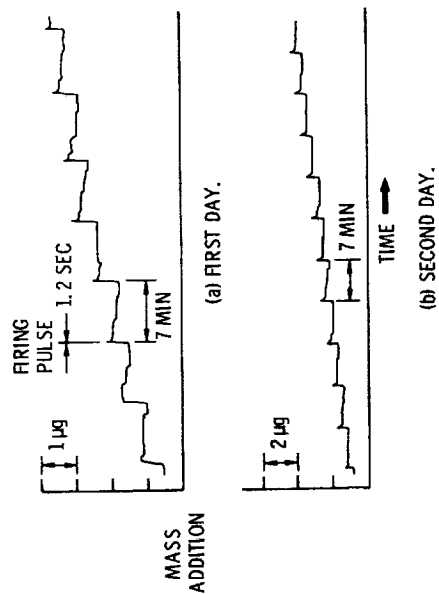


Figure 7. - QCM recorder trace (experiment 1).

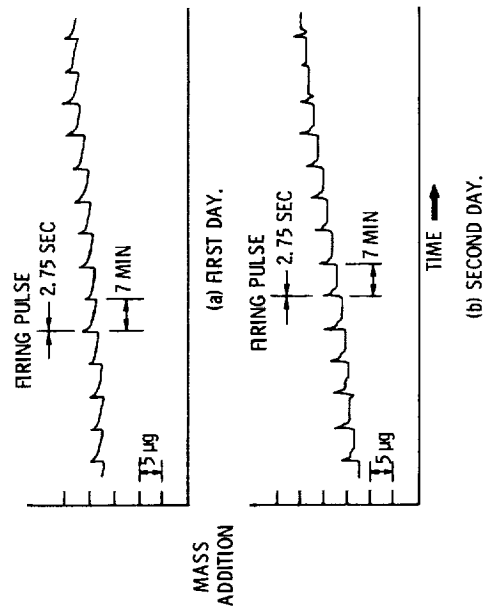


Figure 9. - QCM recorder trace (experiment 3).

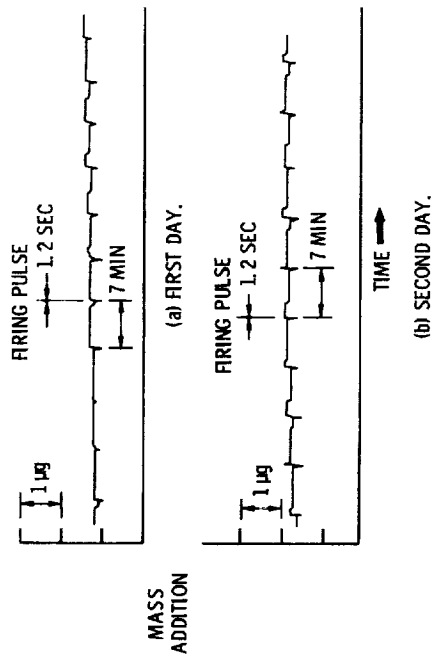


Figure 8. - QCM recorder trace (experiment 2).

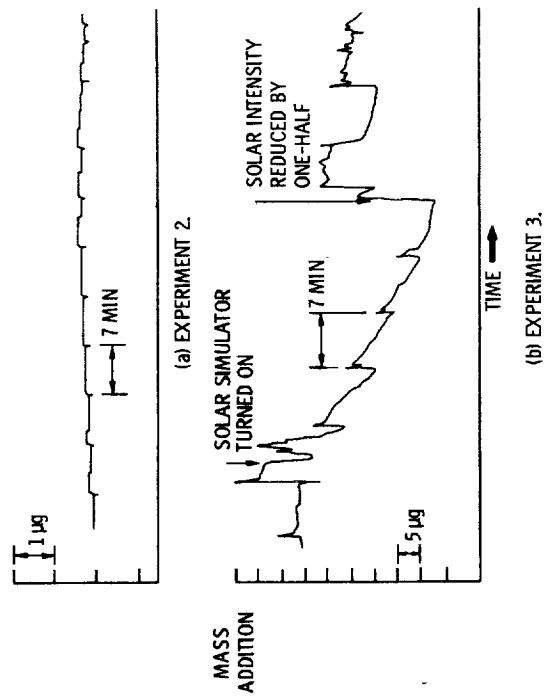


Figure 10. - Unusual events in QCM recorder traces.

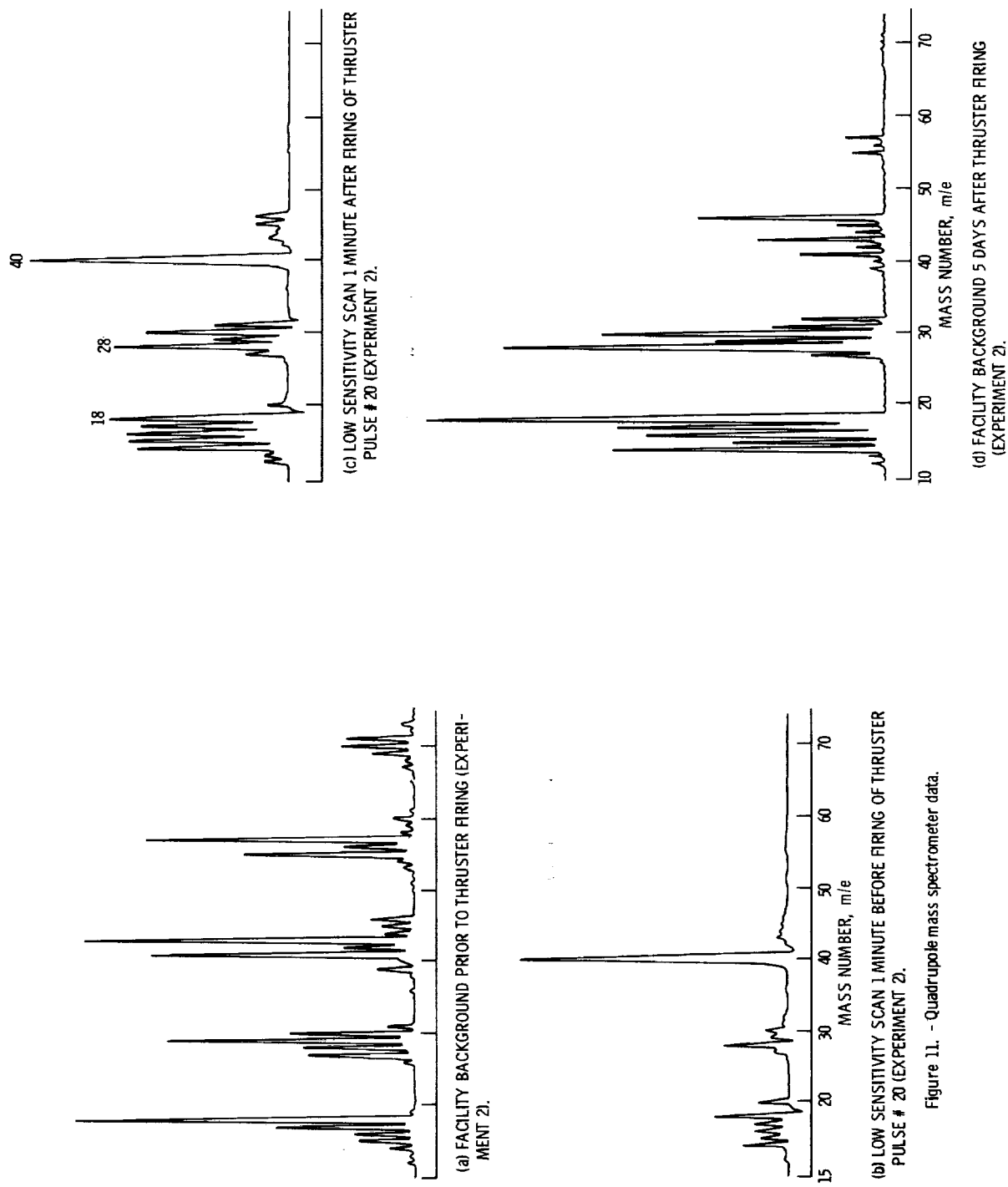


Figure 11. - Concluded.

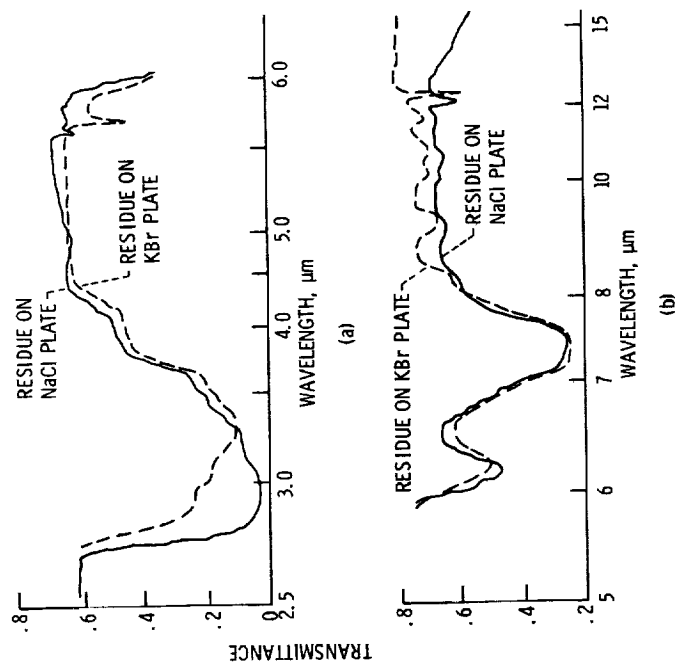


Figure 12. - Infrared spectrometer measurements for residue collected from nozzle (experiment 2).

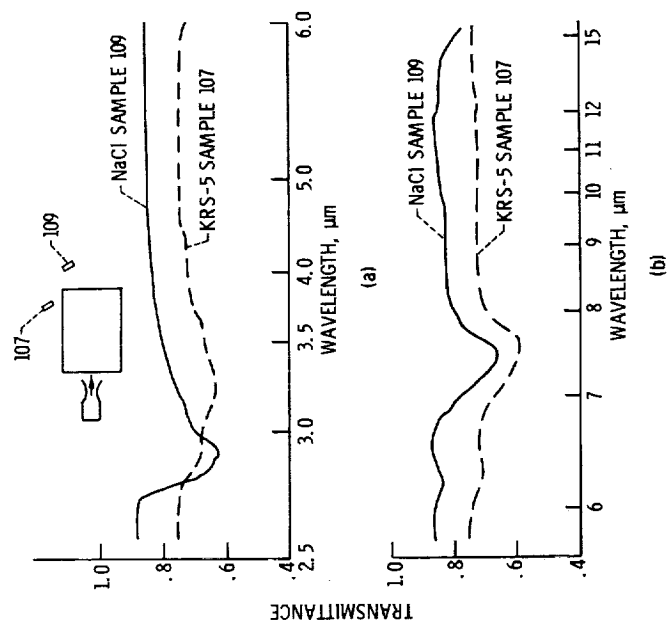


Figure 13. - Infrared spectrometer measurements for contaminated sting-mounted samples in exhaust plume (experiment 2).

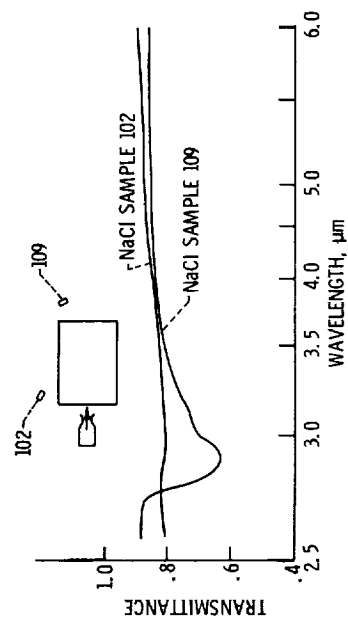


Figure 14. - Infrared spectrometer measurements for contaminated sting-mounted samples in exhaust plume (experiment 2).